EXPANDING HORIZONS: DIVERSE APPLICATIONS OF RUBBERS AND ELASTOMERS IN EMERGING TECHNOLOGIES

Josh N. Bodin,[1] Kuangyu Shen,[1] Songshan Zeng,[2] Luyi Sun[1,3,*]

[1]Polymer Program, Institute of Materials Science, University of Connecticut, Storrs, CT 06269
[2]Macao Institute of Materials Science and Engineering, Zhuhai MUST Science and Technology Research Institute, Faculty of Innovation Engineering, Macau University of Science and Technology, Taipa, Macao, China
[3]Department of Chemical and Biomolecular Engineering, University of Connecticut, Storrs, CT 06269

RUBBER CHEMISTRY AND TECHNOLOGY, Vol. 97, No. 2, pp. 93–117 (2024)

ABSTRACT

Rubbers and elastomers have a rich history that spans many eras of human civilization dating back to 1600 AD. Upon their introduction into Europe, they became common materials in shoes and fabrics. With the invention of vulcanization by Charles Goodyear in 1839, rubbers became widely used in many new applications, ranging from tires to industrial machine parts. Today, rubbers and elastomers are essential in the development of innovative, emerging technologies. This review exemplifies how rubbers and elastomers have been used to advance the emerging fields of soft robotics through soft grippers and dielectric elastomer actuators, stretchable and wearable devices through conductive elastomers and smart elastomers used in thermal camouflage and sensors, biomedical applications through tissue scaffolding and stretch-triggered drug delivery, and energy harvesting through piezoelectric elastomers and wave harvesting triboelectric nanogenerators. This review also briefly summarizes other developments in these fields as well as glimpses into other emerging fields that are advancing through the incorporation of rubbers and elastomers. [doi:10.5254/RCT-D-23-00034]

INTRODUCTION

Rubbers and elastomers, with their remarkable elasticity and flexibility, have a rich history deeply intertwined with human civilization. The story of these materials dates back centuries and is marked by discoveries, innovations, and a growing appreciation for their diverse properties. Historically, their traditional applications have spanned various industries, from transportation to industrial manufacturing, revolutionizing the way we live and work.[1–5]

The earliest recorded use of rubber dates back to 1600 AD in Mesoamerica in the form of sports balls.[1] It wasn't until 1735 that their rubber-making process using latex tapped from *Hevea brasiliensis* trees would be observed and cataloged by Charles Marie de la Condamine of The French Academy of Sciences.[2,3] de la Condamine also reported its use in waterproofing fabrics, shoes, and elastic water bottles as well as its potential use in diving suits. It seemed the possibilities for rubber were endless. Thus, rubber began to see more use in waterproof boots, shoes, and fabrics after it had been brought back to Europe from the Amazon.[4] However, because it cracked in cold temperatures and melted in warm temperatures, its use remained very limited.[1,3,4]

In 1839, American inventor Charles Goodyear overcame these issues, completely by chance, when he mixed rubber with sulfur and dropped it on a hot stove.[2,3] This process created crosslinks between the rubber chains, creating a much improved material that resisted temperature extremes and degradation without compromising its elastic properties.[2,3] Through this process, later known as vulcanization, rubber became a versatile material and saw a new economic boom.[2,3]

With vulcanization, rubber became an essential material in a wide range of items, such as hoses, shoe soles, toys, and insulation. With the Industrial Revolution in full swing, it also found use in new machinery, particularly as a sealant for steam tubes, and as conveyor belts in factories.[2,6] In the late 19th and the early 20th centuries, the birth of the automobile industry created even more demand for rubber as it was used to make tires, shock absorbers, and other components.[2,6]

---

*Corresponding author. Ph: 860-486-6895; email: luyi.sun@uconn.edu

There were many developments of synthetic rubber starting in 1879; however, all were either unusable or too complicated to be used in mass production.[5,7] In 1906, the Bayer company successfully synthesized methyl rubber that was used in World War I as rubber shortages began. However, it was quickly abandoned after the war due to its inferiority and cost to produce.[5] It was finally in 1929 that I. G. Farben discovered that when butadiene and styrene were polymerized in an emulsion and compounded with carbon black, a substance more durable than NR was formed that is known today as SBR.[5,7] This discovery sparked great research into butadiene-based synthetic rubbers with customizable properties, and eventually, the elastomers used today.[5,7]

By the mid-20th century, rubber and elastomers had found their way into a wide variety of industrial applications. Their use as seals and gaskets led to advancements in the aerospace industry, allowing for advancements in design and safety.[8] Today, rubbers and elastomers are commonplace in all manners of products, such as floorings, coatings, machine parts, sealings, tubing, adhesives, sound dampening, and electromechanical instability (EMI) shielding.[8–10]

It seems only natural that their versatility would make rubbers and elastomers prime candidates in advancing emerging technologies. Their exceptional properties, including flexibility, durability, and biocompatibility, have sparked a renaissance in materials science, opening many new frontiers including soft robotics,[11–15] stretchable and wearable devices,[16–25] biomedical applications,[26–29] and energy harvesting.[30–32] Each of these areas represents a unique forefront where the properties of rubber and elastomers have been harnessed to drive innovations that are summarized in this perspective. The Soft Robotics section explores how the inherent compliance and adaptability of rubber-based materials have paved the way for robots that can navigate complex environments, interact with fragile objects, and even mimic biological systems.[33–40] The Stretchable and Wearable Devices section explores the realm of wearable devices, where rubbery substrates and conductive materials blend seamlessly to create flexible devices. These innovations hold the potential to revolutionize wearable technology, healthcare monitoring, and beyond.[41–47] The Biomedical Applications section highlights how rubbers and elastomers have become essential components in medical devices and tissue engineering. These materials offer biocompatibility, flexibility, and durability, all of which are critical attributes in the healthcare industry.[48–53] The Energy Harvesting section exemplifies how rubber-based materials are contributing to the development of sustainable energy sources. From piezoelectric elastomers that can be integrated into many different sensors and devices to triboelectric nanogenerators (TENGs) that can be used to harvest the motion of waves, rubbery materials are playing a pivotal role in the quest for clean and renewable energy.[54–61]

As we explore these new fields, it becomes evident that the diverse applications of rubbers and elastomers in emerging technologies are reshaping industries and opening doors to new possibilities. In this dynamic landscape, we not only reflect on the current state of research but also anticipate future directions and challenges.

SOFT ROBOTICS

SOFT GRIPPER

Traditional hard robots can struggle to grasp regular and irregular objects due to the rigidity of the components. Through the use of elastomers, soft robots with flexible parts can increase friction, making grabbing easier, while also minimizing the damage (a common example of this practice is the rubber-coated handles on tools).

Although coating rubber on metal meets the basic requirements for grippers, more advanced grippers usually have a well-designed structure to achieve extra and enhanced functions. Li et al. developed a unique gripper comprised of three artificial fingers made up of three functional

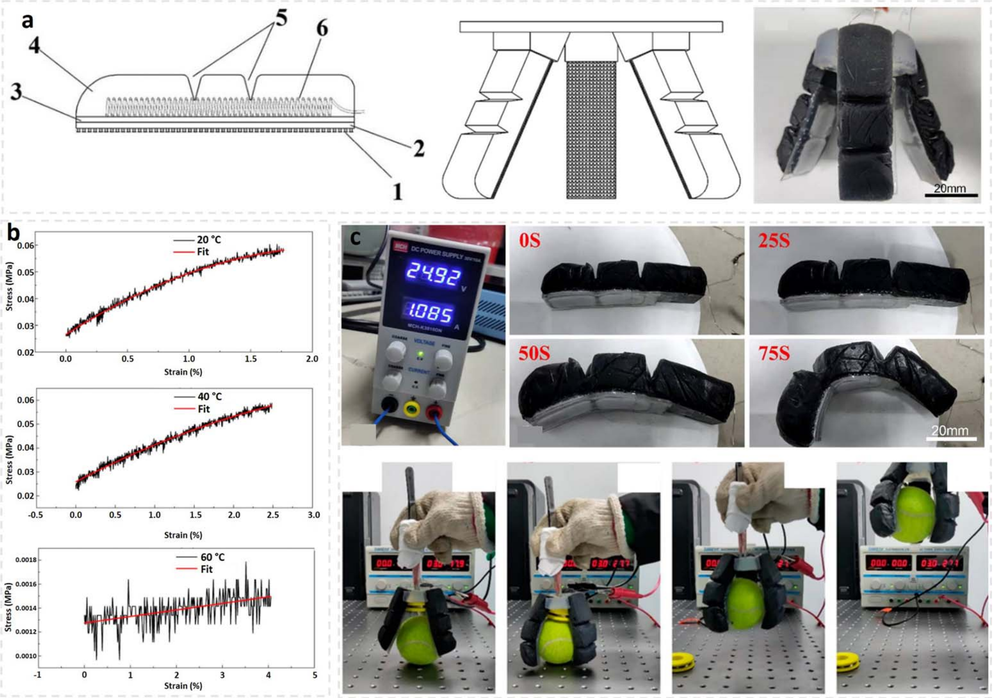

FIG. 1. — (a) General design of the individual fingers with components labeled 1–6 and trifinger gripper: dry adhesive microstructures (1), PDMS supporting layer (2), TPU layer (3), Ecoflex/rGO composite layer (4), V-shape joints (5), and electric wires (6). (b) Stress–strain curves of a single TPU sample over a range of temperatures. (c) Functional testing of a single finger's bending motion and the gripping capability of the final device.[62]

layers to control the stiffness.[62] The upper layer of the trilayered structure was synthesized using a platinum-catalyzed silicone rubber, Ecoflex^{TM}. Part A and Part B of Ecoflex 00-50 were combined in a 1:1 ratio, and reduced graphene oxide (rGO) was added to serve as a heat-conductive filler. A nickel chromium wire was embedded for electrical heating. The middle layer was made of thermoplastic polyurethane (TPU) using commercial TPU powder via compression molding. Polydimethylsiloxane (PDMS) served as the lower layer, as well as dry adhesion microstructures coated on the gripping surface. The upper, middle, and lower layers were then glued together with a thin layer of PDMS and were subsequently cured to form the primary structure of the finger (Figure 1a).

The TPU layer served to give the gripper variable stiffness that allowed bending to occur in response to Joule heating and recovery when left to cool. It showed a nearly linear relationship between stress and strain at different temperatures (Figure 1b). Because of the incorporation of rGO, heat was transferred throughout the finger, allowing a faster bending process. During the actuation, the Joule heating softened the TPU layer and the bending mode could be locked. By controlling the heating process, the mechanical properties of TPU could be retained while grasping objects, but only for a limited time. After turning off power, the Ecoflex/rGO composite began to recover while the TPU remained soft enough to allow bending. TPU became stiffer as it reached room temperature, returning the finger to its initial rigid state. The gripper made up of three artificial fingers was able to successfully grasp three objects—shuttlecock, tennis ball, and beaker—without damaging them (Figure 1c). The total power consumption for the gripper was ~83 W. Although this soft gripper exhibited decent grasping performance, its actuation time (1–2 min) and recovery time (2–3 min) are relatively long, which must be improved for practical application.[62] The TPU-based soft gripper provides a good step toward the potential commercial use of soft robots. Although the total grip and release time is long, the use of thermoplastics with Joule heating opens new avenues to be explored with customized, higher performing materials.

A variety of soft grippers using different types of stimuli and mechanisms have also been explored. Choi et al. developed a soft gripper by using a magnetorheological elastomer skin attached to a robotic gripper, which adapted to the shape of the object and then solidified through the application of a magnetic field.[33] Using a parallel jaw gripper, it was observed that the mechanical properties of the magnetorheological skin could be modulated by adjusting the strength of the applied magnetic field. Furthermore, the controllability of the skin was found to be dependent on the carbonyl iron particle content. The response and recovery times were quantified at 11 and 19 ms, respectively. Notably, the skin demonstrated efficacy in grasping diverse objects, including a cylinder, cuboid, and triangular prism.[33]

Hao et al. used fluidic elastomer actuators to give their soft gripper variable effective lengths while remaining soft and adaptable to the target object.[34] By using a built-in flexible heater, sections of shape memory polymer were softened to facilitate the grasping of objects within a rapid timeframe of 0.6 s. Subsequently, a vortex tube was used to direct jets of cold air, inducing stiffening of the polymer, with a recovery period of 14 s. This dynamic mechanism enables the gripper to adjust its length in response to the object, thereby enhancing the exertion of a higher gripping force.[34]

Self-healing soft robots have also been explored using Diels–Alder polymer elastomers to heal from both microscopic and macroscopic damage. Terryn et al. synthesized self-healing Diels–Alder elastomers, whose healing effects can be activated under the mild heating stimulus.[36] By using this elastomer, macroscopic damage can be healed within 40 min at 80 °C, which can significantly extend the life span of soft grippers subjected to routine wear and tear.[36]

Zhang et al. developed a liquid crystal elastomer (LCE) soft gripper capable of grabbing, moving, and releasing hot objects into cold, safe environments.[63] The LCE foam was fabricated using a salt template method and subsequently developed into a compressible and omnidirectional soft gripper. When the foam approaches a heat source, it begins to contract due to the low thermal conductivity of the foam.[63] Even more improvements can be expected in this ever-growing field in the coming years, with elastomers at the forefront.

ARTIFICIAL MUSCLES

The field of soft robotics necessitates the development of novel soft materials to drive advancements. Although pneumatic actuation stands as the most readily implementable method experimentally, its integration proves challenging in soft robots lacking fixed positioning. Dielectric elastomer actuators (DEAs) have been a major focus point in the field of soft robotics over the past few years. Because of their fast response speeds, high energy densities, electrically induced actuation strains, and mechanical compliance, they are often called artificial muscles. DEAs show potential for a number of soft robot applications.

Shi et al. synthesized a high-performance dielectric elastomer (PHDE) with tunable electromechanical properties through crosslinking and H-bonding within the elastomer network.[64] The PHDE was synthesized using a bimodal network of short and long chain crosslinkers, propoxylated neopentyl glycol diacrylate (PNPDA) and CN9021 (a urethane diacrylate), respectively. The long chain segments ensured large elongations, and the short chain segments increased the modulus at moderate strains. Butyl acrylate and isobornyl

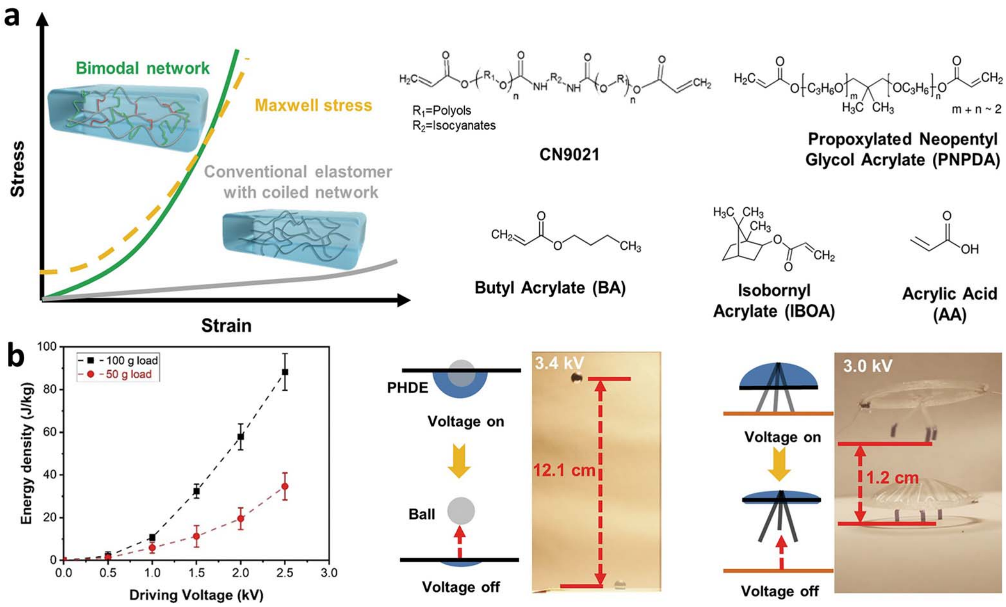

FIG. 2. — (a) Design of the PHDE. (b) Electrical properties testing.[64]

acrylate were selected as comonomers to lower the modulus and improve toughness. Stress–strain responses and viscoelasticity were tuned using various methods. First, short chain crosslinkers were used in lieu of short, stiff additives to tune stretchability and tensile strength, whereas the stress–strain responses and crosslinking density were controlled by changing PNPDA concentrations. Second, the viscoelasticity was controlled by optimizing the hydrogen bonding content through the addition of acrylic acid (AA).

The PHDE was made using a moderate ratio of short-to-long chain crosslinker that was found to be ideal for high actuation strains (Figure 2a). At 10 wt% PNPDA, a maximum strain of 189% was achieved while fully suppressing EMI. After adding a small amount of AA, viscoelasticity was reduced leading to quicker response time while maintaining high and stable actuation. The resulting PHDE showed high dielectric strength with an apparent electrical breakdown field of 330 V/μm, low leakage currents, a high dielectric constant of 5.35, and a small dielectric dissipation factor of 0.014 at 1 kHz. Under preloaded conditions, the PHDE outputs a stable force of ~0.95 N at 2.5 kV with a 1.2 N preload, without the need for pre-stretching. Under isotonic conditions, the PHDE films performed specific work of ca. 35 and 88 J/kg for 50 and 100 g loads, respectively, at 2.5 kV (Figure 2b). In addition, with a 100 g load, the PHDE films maintained energy densities of ca. 67 and 18 J/kg at 5 and 20 Hz, respectively. The corresponding power densities were calculated to be ca. 670 and 640 W/kg. However, at frequencies >50 Hz, the films could not efficiently perform work. A dry stacking method for multilayered DEAs was developed to improve the energy and power outputs at low voltages.

The process proved to be very efficient because film preparation, electrode deposition, and lamination can be conducted in parallel. The process became even more efficient by dry stacking PHDE layers on one another (Figure 3a). A 10-layer PHDE actuator showed comparable strain actuation to a single-layer actuator at the same low driving voltage (Figure 3b). High response speeds were found for the multilayered actuator while achieving strains of ~110% at 2 Hz and ~60% at 20 Hz. The number of layers used in the dry stacking method can linearly scale

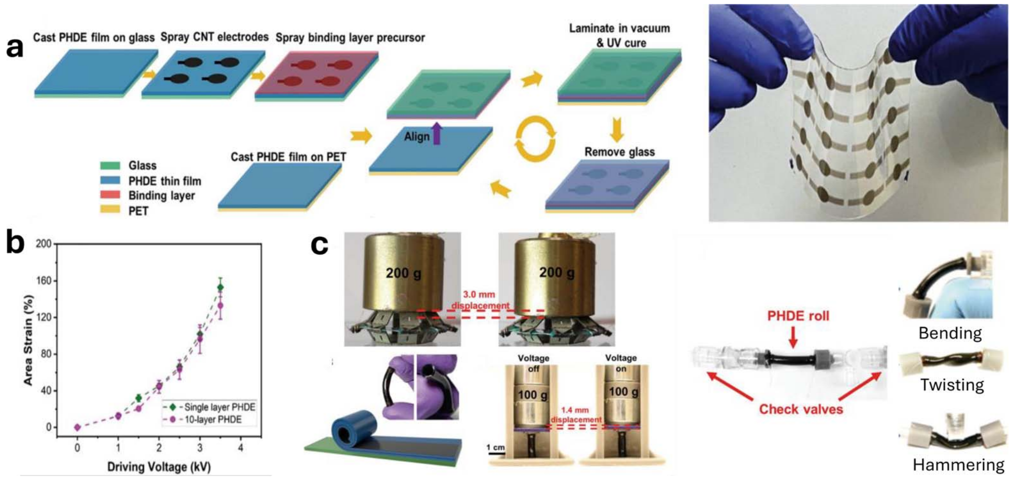

FIG. 3. — (a) Fabrication of a PHDE actuator by using dry stacking method and 10-layer PHDE actuator. (b) Static actuation test and frequency response. (c) Testing of PHDE spider and rolled actuator.[64]

up the force and energy outputs with increasing driving voltage while experiencing a <20% reduction with each new layer. The dry stacking method also allowed for new actuator designs, such as a spider actuator that successfully lifted a 200 g load with ~3.0 mm linear displacement at 2.5 kV with a specific work of ~74 J/kg. A roll actuator was also designed using the new dry stacking method. It was able to lift a 100 g load by 0.64 mm at 0.5 Hz, with an output energy density of 15.6 J/kg. Aside from a small amount of conductive materials, the roll actuator was entirely polymeric, allowing it to function even after twisting, bending, and sustaining impact (Figure 3c). The roll actuator was further modified into a tubular pump by integrating two check valves. By varying the driving voltage and frequency, the flow rate can be controlled, reaching a peak flow rate of ~20.4 mL/min at 2.5 kV and 10 Hz, making a specific flow rate of ~100,000 mL/kg per min.[64] This elastomer allows for low-voltage actuation without the need for any hard components, which opens the path for many different flexible technologies in soft robotics. In addition, the output can be increased through modular stacking while maintaining a relatively low driving voltage. This versatility extends the applicability of the technology to a broader range of contexts and industries.

Elastomer actuators have been explored for many different applications. One such application was for four-dimensional printed LCE actuators, where the LCEs were printed into complex three-dimensional (3D) shapes that could undergo controlled shape changes with tunable actuation temperatures and strains. Saed et al. used direct ink write to control the direction of molecular order to be along the print path, leading to LCEs with ultralow actuation temperatures.[38] Further control of the physical properties can be achieved by varying the spacer, crosslinker, or mesogen concentration of the LCE.[38] Zadan et al. used LCEs with embedded semiconductors and liquid metal interconnects to cyclically heat and cool the elastomer to induce actuation.[39] This actuator can use the internal temperature differentials between the LCE layers to trigger the Seebeck effect, converting the thermal energy into electrical energy that can be used in subsequent actuation cycles. The resulting thermally driven actuator becomes incredibly energy efficient as it generates energy with each actuation.[39]

DEAs were also used to develop a wearable soft haptic communicator. Zhao et al. created a two-by-two soft actuator array from the DEAs that can be worn on the arm to keep the hands free.[40] Because of the use of DEAs, the haptic device can be worn for long periods of time

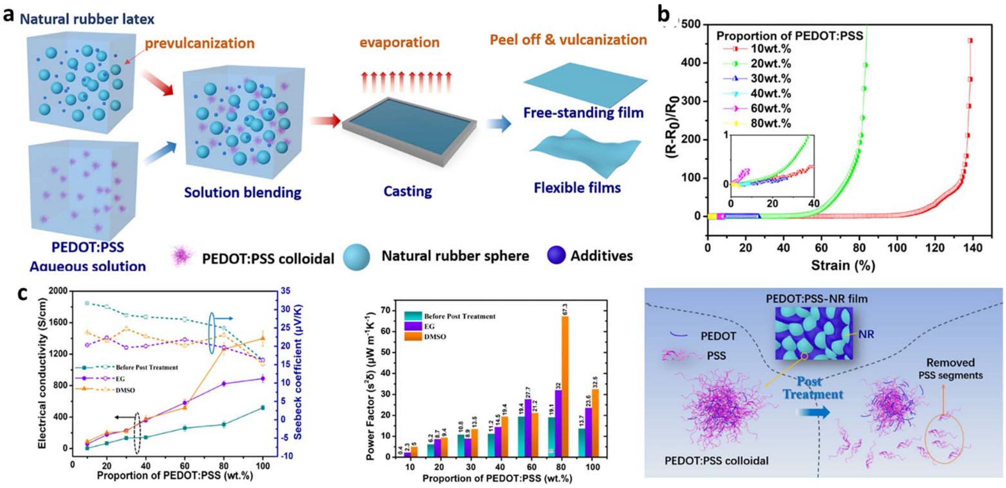

FIG. 4. — (a) Preparation process of NR/PEDOT:PSS film. (b) Rate of resistance changes under stretching and curves under various strains. (c) Electrical conductivity and Seebeck coefficient testing, power factor of post-treated films, and schematic diagram of the secondary doping principle.[66]

without causing the wearer fatigue, as well as having better adaptability than currently existing devices that use hard components.[40] Liang et al. developed an elastomer that could grow automatically without the need for external stimuli after pre-strain has been installed.[65] When growth starts, it will keep going even after the force is removed. Very few materials can undergo such behavior, and those that do show an unusual liquid crystal phase. Current results for these LCEs are limited; however, once growth speeds in the material can be controlled, multiple self-elongating LCEs can be assembled into complex actuators with low energy requirements.[65] Overall, elastomer actuators are expected to play a major role in soft robotics in the future.

STRETCHABLE AND WEARABLE DEVICES

ELASTIC CONDUCTOR

Flexible electronics prove to be the next major step in developing wearable devices, and by extension, vastly improved sensors for health monitoring. With the growing interest in flexible electronics, stretchable conductors made from rubbers and elastomers have become an essential research area in making them a reality.

Yang et al. improved upon NR by incorporating it with conductive copolymer poly(3,4-ethylenedioxythiophene) polystyrene sulfonate (PEDOT:PSS) to improve its conductivity.[66] NR/PEDOT:PSS films were prepared by first making a dispersed solution of natural latex rubber and then a separate solution of aqueous PEDOT:PSS with 5 vol% ethylene glycol (EG). The aqueous PEDOT:PSS solution was adjusted to a pH of 8 through the addition of $NH_3{\cdot}H_2O$. Next, the natural latex rubber solution was added dropwise into the PEDOT:PSS solution under mild stirring and ultrasonication, and this solution was subsequently degassed and vulcanized (Figure 4a).

As the PEDOT:PSS content was increased, the elastic modulus and elongation at break of the resultant NR/PEDOT:PSS composite both decreased. When it exceeded 20 wt%, the material was brittle. It is believed that when PEDOT:PSS is in high content, it blocks the bonding between NR particles, greatly lowering the elongation. As PEDOT:PSS content was increased, the electrical conductivity also increased, but the Seebeck coefficient decreased. When a higher content of elastomer was blended into PEDOT:PSS, it not only improved the stretchability but also yielded higher thermoelectric voltage than the neat PDEOT:PSS. This effect is due to the insulating properties of NR having an energy filtration effect on the carrier migration of PEDOT:PSS that, in turn, raises the Seebeck values that are inversely proportional to the carrier concentration. The power factor value was found to be mostly dependent on electrical conductivity, reaching its maximum at 60 wt% PEDOT:PSS. The general trend of the NR/PEDOT:PSS composite films with differing PEDOT:PSS contents was that $(R-R_0)/R_0$ (where R is the resistance when stretching and R_0 is the initial resistance) increased with an increasing strain until fracture (Figure 4b). For the NR/PEDOT:PSS composite containing 10 wt% PEDOT:PSS, the variation in resistance was small, within a range of 0–90%, and this change was likely attributed to the change in length and cross-sectional area of the spline during stretching.

The gauge factor (GF) value was found to be 3, with most conventional conductive metals having a value range of 2–5. This shows conductive stability under a small strain range. At higher strain ranges of 90–130%, $(R-R_0)/R_0$ sharply increased as the material cracked under a large deformation. For the composite films containing 10 and 20 wt% PEDOT:PSS, the voltage–current relationship was linear under different strains, indicating relative stability under certain strains. In 0–10 and 0–50% strain cycles, the tensile sensitivity GF values were low at 0.2 and 0.5, respectively, whereas 0–100% strain cycles showed significant changes in resistance. Through testing, it was found that PEDOT:PSS lost the ability to bear tensile stress after two stretching cycles, causing deformation and a lower elastic modulus. To compensate, spherical NR particles were interlaced and bonded together on the composite film's surface to form grooves and folds that helped increase the film's toughness. At 50% strain, the rubber particles were stretched into fibers and cracks began to appear. At 100% strain, the particles were even further elongated and more cracks appeared, which destroyed the PEDOT:PSS conductive pathway.

NR/PEDOT:PSS films were post-treated via immersion in EG (99%) or dimethyl sulfoxide (DMSO; 99%) at 60 °C for 30 min. Post-treatment was used to improve the overall performance, especially the thermoelectric and electrical conductivity properties. The X-ray photoelectron spectrometer characterization results indicated that PSS was selectively removed during the post-treatment process, allowing PEDOT to expose and overlap one another, thereby improving the conductivity. The EG treatment was found to alter the film from ductile to brittle, whereas the DMSO-treated films maintained ductile mechanical properties. Using post-treatment methods with EG and DMSO, electrical conductivity was able to increase dramatically while decreasing the Seebeck coefficient slightly. An NR/PEDOT:PSS composite (containing 10 wt% PEDOT:PSS) film after EG post-treatment saw an increase in electrical conductivity from 4.1 to 56 S/cm and a Seebeck coefficient decrease from 31 to 20 μV/K. After treatment with DMSO, its electrical conductivity increased to 87 S/cm and the Seebeck coefficient decreased to 24 μV/K (Figure 4c). Overall it was found that DMSO was the best secondary dopant because it not only improved the conductivity but also maintained the tensile properties. The composite film showed self-healing capabilities when exposed to water. A sample stretched to 100% saw an unrecovered strain of 17%, a resistance change rate of 4.2, and $(R-R_0)/R_0$ of 3.8 upon stress release. When immersed in water and phosphate-buffered saline (PBS) for a while and left to dry, the unrecovered strain decreased to 0.8%, the resistance change rate to 0.2, and $(R-R_0)/R_0$ to 2.1. As previously discussed, 100% stretching destroyed the conductive phase, causing broken fragments to appear on the sample surface. In addition, microcracks formed on the surface. When the sample was treated with water, the surface became smooth again, due to the swelling of PEDOT:PSS causing lapping of the cracks, and the hydrogen bonding of the PSS healing those cracked as it dried, thereby restoring irreversible deformation and electrical properties. The resistance of the DMSO-treated NR/PEDOT:PSS (containing 10 wt% of PEDOT:PSS) was tested under bending, twisting, folding, and multiple bending conditions. For all tests, the resistance was found to be ca. 3 Ω for all testing conditions, indicating the materials can be used in flexible conductors.[66] This elastomer combines the favorable stretchability of NR with the notable conductivity of PEDOT:PSS to create a stretchable and bendable material capable of conducting electricity. Furthermore, it can heal from cracking and deformation through the addition of water, opening the door to the next generation of wearable technology.

Flexible conductors are a necessary component for the next generation of emerging technologies. As such there have been countless studies to further their properties and applications. For example, Jiang et al. developed an elastic conductor made from PDMS and gold nanoparticles (NPs) with a thickness of 1.3 μm for breathable, and water-resistant, on-skin electrodes.[67] The resulting device was capable of continuously recording electrocardiogram signals during daily life as well as strenuous exercise.[67] Another study developed a printable fluoro-elastomer containing silver flakes with both high conductivity and stretchability, promising to be used in electronic textiles. Using a fluoro-elastomer, Matsuhisa et al. created highly conductive and stretchable conductors through a one-step printing process that was used to create a textile EMG-measuring device.[68] The device was found to have a maximum gain of up to 290 kHz and a cutoff frequency exceeding 1 kHz, which proved sufficient for its intended use.[68]

Similarly, a conductive elastomer made from TPU and silver nanowires was developed that could be easily printed onto textiles with sufficient washability. Zhu et al. used silver nanowires and a TPU ink in a one-step printing process to produce e-textiles that were conductive, with a reported conductivity of 3,668 S cm^{-1}; showed over 100% stretchability; and due to high bonding force, maintained high conductive stability even after 20 consecutive wash cycles.[69] Wu et al. developed an ionic conductive elastomer through the copolymerization of thioctic acid and hydroxyethyl acrylate that could be fabricated through a solvent-free synthesis.[70] The presence of disulfide bonds enables self-healing abilities in addition to its conductive properties. The final elastomer showed high transparency, with a 94% transmittance within the range of 500–780 nm; stretchability of 473% strain; and conductivity up to 10^{-4} $S{\cdot}m^{-1}$. In addition, it showed high recyclability, giving it high promise for use in future flexible technologies.[70] Elastic conductors will undoubtedly be a major milestone in technological advancement.

STRETCHABLE DEVICES

Elastic conductors show the most practical use when used in stretchable and flexible devices that can be worn on the body, as current conductive materials tend to break under too much strain. Although stretchable devices are largely affiliated with flexible sensors, there are many other types of stretchable devices with unique uses. The stretchable properties of elastomers allow for many applications to be explored such as thermal camouflage.

Zeng et al. took inspiration from cephalopods to develop strain-based thermal camouflage.[71] A uniform layer of polyvinyl alcohol (PVA)/laponite layer was cast using a PVA/laponite aqueous dispersion that was then treated with allyl isocyanate. Ecoflex 00-30 was cast on the treated PVA/laponite film and cured. The bilayer film was then peeled away from the foundation in a singular direction to promote distributed cracks. Mirrored chrome (MC) was then spray coated onto the PVA/laponite layer. A heater was incorporated through the addition of a conductive thread in a serpentine pattern attached to a circular very high bond tape, with a polystyrene disc at the bottom (Figure 5a).

The experimental heat flux emitted by the device was tested via sensor complex and thermocouple temperature measurement. Heat flux showed progressive growth from 68.7 to 112.6 W/m^2 as the uniaxial strain increased from 0 to 150%. The thermocouple results showed

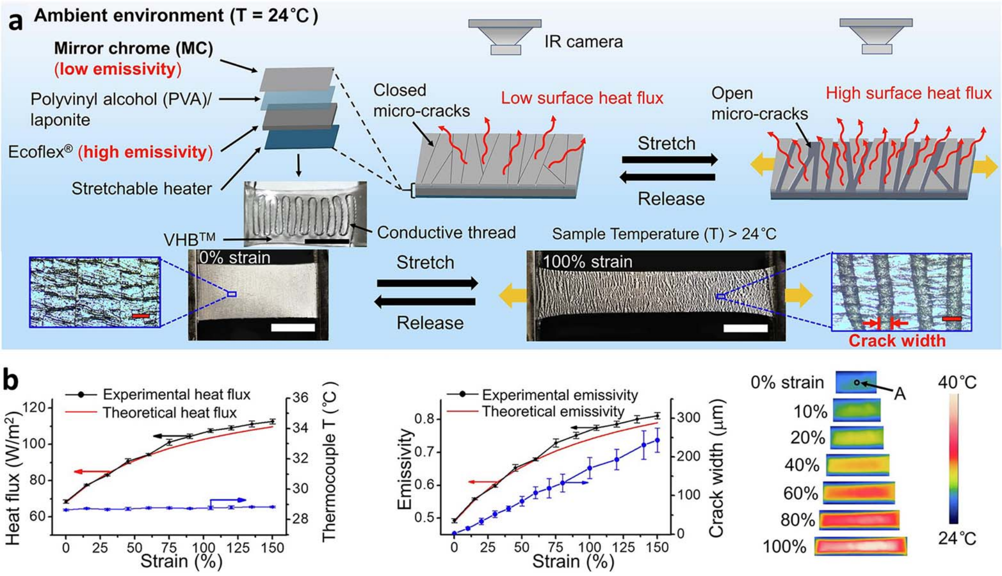

FIG. 5. — Schematic (a) and characterizations (b) of thermal device.[71]

no change and remained at 28.7 °C. The average crack width increased to 33.4, 132.9, and 243.5 μm at 20, 80, and 150% strain, respectively, whereas the emissivity increased from 0.49 at 0% up to 0.81 at 150% strain (Figure 5b). The heat flux of the device showed instantaneous, reversible, and synchronized response under multiple stretch–release cycles of 50% strain/s (with the maximum strain of 150%) without recognizable hysteresis. Under thermal camera imaging (TCI), the heated device appeared blue-green at 0% strain ($T_{rad} = 24.7$ °C), and changed to yellow at 20% ($T_{rad} = 26.8$ °C), red at 60% ($T_{rad} = 30.1$ °C), and red-white at 100% strain ($T_{rad} = 34.4$ °C). Because of the thermal radiation being omnidirectional, it allowed for observation angle independence from the TCI. In addition to the above-mentioned manually stretchable device, a pneumatic actuation system was also developed, where the MC, PVA/laponite, and Ecoflex layers act as a deformable, circular diaphragm with a substrate containing a heater and were connected to a tube to inflate and deflate the diaphragm. When inflated the device bulges and expands into a spherical shape, which causes the distributed cracks on the thin film to open and expose the substrate (Figure 6a). The heat flux increased from 71.3 to 108.4 W/m^2 from 0 to 100% strain. The crack area ratio increased with an increasing strain, causing the emissivity to increase from 0.51 to 0.78 over the same strain range. This device also showed excellent reversibility under multiple inflation/deflation cycles. Because it can be controlled to tune its surface emissivity, it can be used in autonomous camouflage under a thermal camera. When placed in a cool area ($T_{rad} = 32.2$ °C) appearing as yellow under TCI, the device was able to become completely invisible by inflating to 31.8% strain to reach the same T_{rad}. When moved to a hot area ($T_{rad} = 36.4$), appearing as red under TCI, the device was able to camouflage itself again by inflating to 64.9% strain to match the T_{rad} (Figure 6b). This process could be repeated many times, showing its capabilities as an adaptive and autonomous soft thermal camouflage device.[71] This device establishes a new type of camouflage that allows the user to blend into their thermal surroundings.

Although most stretchable devices refer to wearable sensors, there are a variety of other devices that have been realized. For example, a supramolecular water-assisted self-healing polymer (WASHP) was developed and successfully used in a light-emitting, touch-responsive underwater

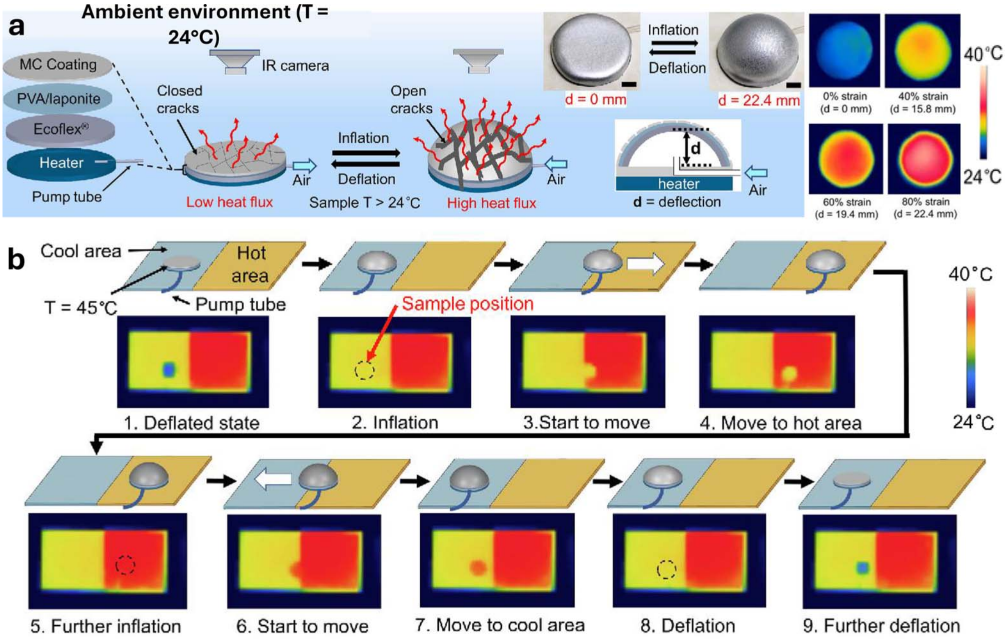

FIG. 6. — (a) Schematic and characterizations of thermal modulating system for bulging strain (TMSB). (b) Design and performance of TMSB thermal camouflage device.[71]

device. He et al. reported that their WASHP had a self-healing time of 1 h, with a self-healing efficiency of 95%.[41] The resulting light-emitting, touch-responsive device showed good adhesion even on rough surfaces, as well as controlled luminescence, even under strain.[41] Souri and Bhattacharyya used straightforward fabrication techniques to develop a wearable elastomer/cotton heater using graphene and carbon black.[42] They first sonicated trimmed fabrics in a solution comprising graphene nanoplatelets and carbon black NPs. Subsequently, these treated fabrics were incorporated into molded Ecoflex to craft a wearable heater. Notably, the resultant device achieved a maximum temperature of 103 °C by using 20 V.[42]

Electronic skin has also been thoroughly investigated within wearable devices, with one group reporting a highly robust, self-powered e-skin by using the triboelectric-electrostatic induction effect and self-healing abilities of polyurethane elastomers. Xun et al. used carbon black–doped conductive polyurethane elastomer covered with nonconductive polyurethane elastomer to create an e-skin possessing a triboelectric effect.[43] The e-skin showed microscale healing abilities with full restoration after 24 h. Deshmukk et al. synthesized a stretchable substrate from butyl rubber and barium strontium titanate (BST) for use in wearable devices.[72] The elastomer underwent phenolic curing to maintain conductivity, as opposed to sulfur curing that resulted in nonconductive inks. It was found that the maximum BST filler was 40% by volume, with elongations >200%.[72] Wearable devices are an achievable goal, and as elastomers are improved, they will improve along with them.

SENSORS

Wearable sensors represent a significant focal point within the realm of wearable devices, offering immense potential for detecting various stimuli through a range of methodologies.

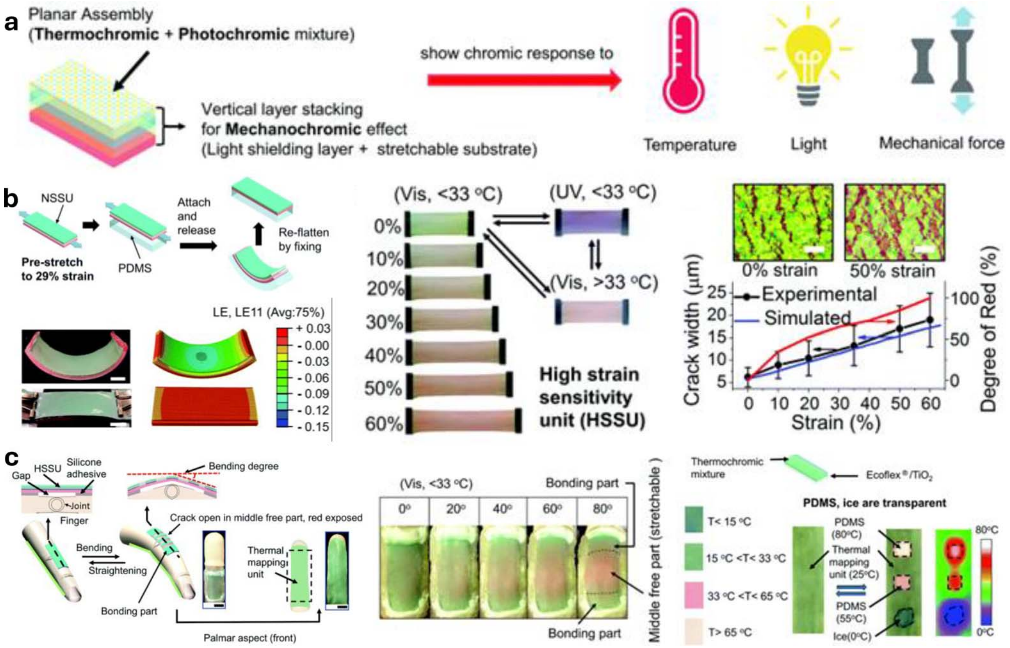

FIG. 7. — (a) Preparation schematic of the MSR device. (b) Design and performance of the device. NSSU, normal strain sensitivity unit. (c) Performance of the wearable motion monitor.[73]

Motion sensors with responses to multiple stimuli, particularly, have been a key area of research for years. The soft and flexible properties of elastomers make these devices achievable where other materials fell short, allowing for a variety of sensing methods such as piezoresistive and mechanochromic sensing.

Sun and coworkers developed a multistimuli responsive (MSR) material that can be integrated into a strain-based sensor to monitor bending and environmental stimuli through color change.[73] The thermochromic and photochromic properties of the MSR units can be achieved by homogeneously mixing powders with the appropriate color-changing style and mass ratio. The colorimetric thermal mapping unit can be similarly made by mixing different thermochromic pigments. Finally, mechanochromic characteristics can be introduced by adding a rigid photochromic/thermochromic film on a light-shielding layer that is attached to a stretchable substrate. This creates a device that, when stretched, causes distributed cracks to appear on the top rigid layers (Figure 7a). This allows for adjustable exposure to the soft substrate layer through pre-stretching crack distribution and gives the device color-changing properties under strain.

The high strain sensitivity unit (HSSU) showed higher mechanochromic sensitivity than its normal strain sensitivity unit counterpart, with color change occurring instantaneously at ca. 20% strain. The HSSU could be further integrated into a wearable motion/environmental monitoring (WMEM) device to measure finger bending and other related conditions, with the deformation localizing on the joint when the finger is bent (Figure 7b). The WMEM includes a thermo-mapping unit using three types of thermochromic pigments with different critical transition temperatures. The colors change based on the temperature range. At temperatures <15 °C, it appears blue; at a temperature range of 15 to 33 °C, it is green; at temperatures between 33 and 65 °C, it appears red; and at temperatures >65 °C, it is white. The WMEM also showed accurate mapping ability with the thermochromic contour matching the shape of the target object. When the finger is bent at 40 °, the middle free part of the HSSU becomes red and distinguishable from the rest of the material, which stays green. At 80 °, bending the red area reaches maximum intensity (Figure 7c). A smartphone colorimetric analysis app was further introduced as an easy analysis method. The app captures the color change and converts it to the corresponding bending angle via the screen. As the bending degree increased, strain levels and degree of red (DR) both increased proportionally, to a maximum strain of 26.9% and a maximum DR of 100% when the finger was bent to 80 °.[73] This sensor changes colors in response to bending, as opposed to other sensors that typically generate an electric charge. This allows for strain monitoring without the need for any special equipment and with no delay between stimuli and response.

Wearable sensors prove incredibly useful in the medical field. Because certain issues need to be monitored, a variety of sensors with different responses to stimuli have been developed. Liu et al., inspired by the high flexibility of spider webs, created a strain sensor from elastomer-filled graphene woven fabric, which is highly flexible and transparent.[45] A wearable sensor was created by using graphene woven fabric with an elastomeric PDMS core. The resulting sensor demonstrated the ability to detect finger and neck motion as well as tiny vibrations caused by pronouncing different letters.[45]

Li et al. developed a highly sensitive and stretchable sensor from ultraviolet/ozone (UV/O_3) cracked elastomer/carbon nanotube (CNT) composites that can detect various motions, from the movement of the wrist to the blink of an eye.[44] The sensor operates on a UV/O_3 cracked elastomer composite containing CNTs. The enhancement in sensitivity, with a remarkable GF of 1020.2, is attributed to the expansion of cut-through cracks induced by UV/O_3 exposure. This innovative approach enables the sensor to detect various motions, such as wrist bending, pulse, and blinking, thereby demonstrating its versatility and efficacy.[44]

Tan et al. developed a sensor with excellent heat dissipation properties by using a TPU/boron nitride nanosheet composite, graphene nanoribbons, and porous electrospun fibrous TPU. While maintaining excellent stretchability and sensitivity, the heat dissipation properties help prevent thermal damage to the device, and more importantly, the wearer.[47]

Peng et al. improved upon vat polymerization 3D printed self-healing polyurethane elastomers, which tend to have low tensile strength, by using dynamic hindered urea bonds.[74] With the addition of surface-functionalized spherical nano silica, the tensile strength and elongation at break both saw improvement. This modified elastomer was then incorporated with ionic liquids to ultimately be used to print a pyramid-Kelvon lattice microstructure pressure sensor. The combination of 3D printability and the self-healing nature of the elastomer offered more structural freedom in designing and fabricating wearable sensors.[74] Needless to say, elastomer-based sensors have demonstrated rapid growth in recent times.

BIOMEDICAL APPLICATIONS

CONTROLLED DRUG RELEASE

Similar to sensors, elastomers and rubbers can be used as a form of controlled drug release under certain conditions, such as bending and stretching, and can be customized to control the amount and the period over which they are released. Drug delivery elastomer devices can make necessary regular injections, such as of insulin, as easy as bending one’s finger, and design them to deliver specified amounts even under constant stretching.

Di et al. developed a simple, stretch-activated drug delivery system using an elastomer containing microdepots filled with drug-containing NPs.[75] The microdepot integrated device was

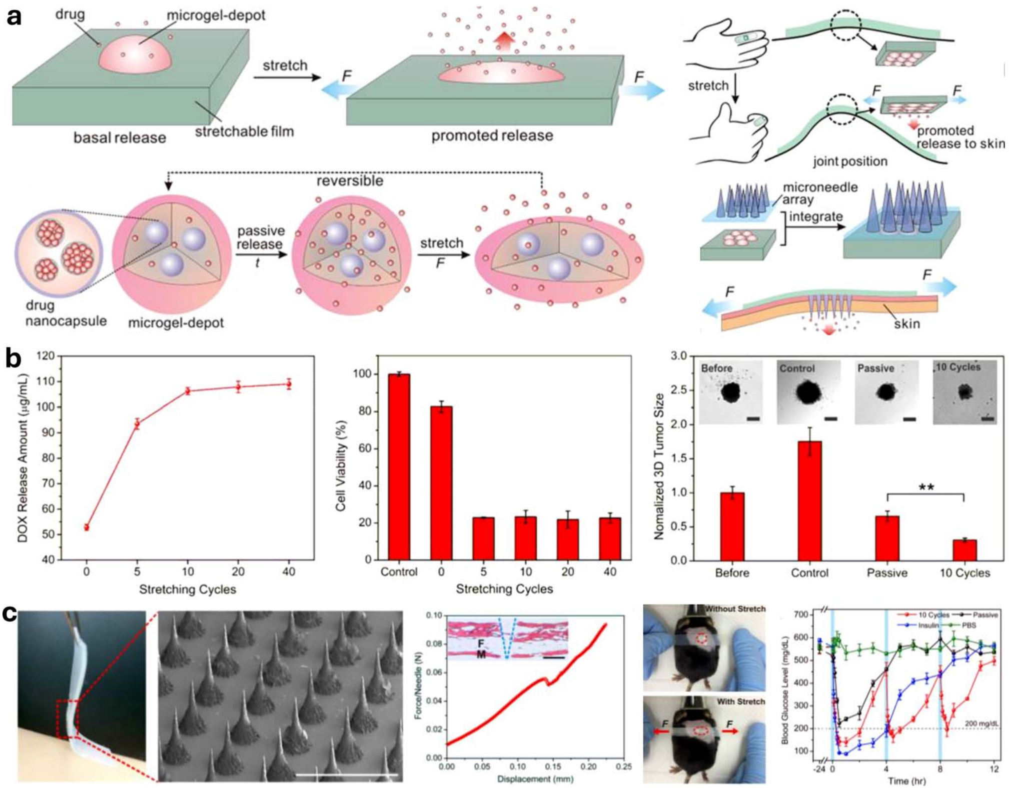

FIG. 8. — (a) Schematic illustration of the tensile strain-triggered drug release. (b) In vitro anticancer effects and bactericidal applications of the wearable device. (c) In vitro and in vivo studies of the stretch-mediated blood glucose (BG) level regulation for STZ-induced diabetic mice by using microneedle integrated device.[75]

prepared by coating a layer of self-sticky silicone onto a glass slide, followed by a layer of Dragon Skin^{TM} 30 that was selected as the elastomeric substrate due to its commercial availability, high performance, large stretchability (up to 360%), and ability to cure at room temperature. A 5 mm diameter biopsy punch was used to punch a circle in the middle of the elastomer. The area was then filled with liquid Dragon Skin 30 precursor that was pre-cured at room temperature before adding drug-containing microdepots. The liquid was then fully cured at room temperature, thereby half-embedding the microdepots into the elastomer (Figure 8a). The microneedle integrated device was made using five silicone molds with an array of 11 × 11 conical cavities. Hyaluronic acid (HA) was modified with methacrylated pendants and then mixed with Irgacure-2959 (photo-initiator) and *N*,*N*-methylenebis(acrylamide) (crosslinker). The mixture was then deposited into the molds and vacuum dried. Afterward, the arrays were UV crosslinked.

The chemotherapeutic drug doxorubicin hydrochloride (DOX) was used as a model drug during testing. To encapsulate DOX, poly(lactic-co-glycolic acid) NPs were prepared via a double emulsion–based solvent evaporation/extraction method. The NPs were encapsulated in alginate microgels via electrospray and then crosslinked with barium chloride. The microdepots were measured at 406.2 ± 14.5 μm in diameter. The embedded microdepots followed geometric changes to the substrate upon stretching and recovered with slight residue deformation. The microdepot embedding depth can be adjusted through the pre-curing time of the elastomer. Microdepots were mounted to a stage and underwent 10 cycles of 50% strain with a frequency of

0.5 Hz to quantify drug release. Shallower embedding depths under longer pre-curing times led to higher volumes of microdepots surrounded by PBS. The released drug amounts increased with pre-curing time up to 30 min. This corresponds to the spherical microdepots being half-embedded into the substrate. Release amount also increased with increasing strain, with 75% strain showing the highest release amount. However, most human motions do not exceed 50% strain. The last crucial factor in the release amount is the time between stretching events, due to the slow rate of diffusion of the drug from the NPs to the microdepots. It was found that 4 h was sufficient for the drug to replenish into the microdepots.

Sample solutions from devices that underwent stretching showed higher cytotoxicity than those that had not. Sample solutions from stretched devices were shown to significantly reduce the size of the tumor with loose intercellular junctions after 3 days compared with sample solutions from unstretched devices. Enhanced drug delivery under stretching can be attributed to an enlarged surface area of the microdepot in contact with the aqueous solution and the Poisson's ratio–induced compression on the microdepot. To test body motion for drug release in the stretch-mediated devices, the antibiotic ciprofloxacin was incorporated into the device for sustained treatment of local infection. The device was attached to the finger with the microdepots making conformal contact on the joint. When the finger was bent, the device was stretched, facilitating drug release. It was found that drug release amount and bacterial killing areas both significantly increased with the number of bending motions (Figure 8b). Traditional insulin injections for type 1 and advanced type 2 diabetes require injections several times a day. This can cause infection, tenderness, nerve damage, and tissue necrosis. However, with an insulin-containing microdepot device integrated with microneedles made from crosslinked HA, these issues can be avoided. The in vivo performance of the device was proved to be very effective on streptozotocin (STZ)-induced type 1 diabetic mice (Figure 8c).[75] The elastomer-based drug delivery device is stretch activated, making it easy to use during daily life. In addition, the use of a microneedle array eliminates the adverse effects associated with the frequent use of standard-sized needles. This innovation holds particular promise for children requiring frequent injections, as it addresses potential aversions or discomfort they may experience.

Wearable drug delivery systems can provide huge improvements to those who need regular injections in everyday life. Many designs and materials have been investigated to improve upon the technology. One way of doing this is through 3D printing to make a more customized device making use of a novel, nonbiodegradable polyester-based thermoplastic elastomer that is highly 3D printable and biocompatible. Koutsamanis et al. developed a multiblock alternating copolymer made of semicrystalline polybutylene terephthalate hard segments and poly-ether-terephthalate amorphous soft segments.[51] The novel elastomer was then used to make a drug delivery device via 3D printing with a fine-tuned surface area to control the daily released drug amount.[51]

In another example, a hydroxyl-dominant polydiolcitrate elastomer was synthesized for use in a thermally induced shape memory device, with an active range from room to body temperature, that can slowly release small molecules. By using a hydrophobic diol and making a minor increase in the hydroxyl-to-carbonyl mole ratio of poly(1,12-dodecanediol-co-citrate), Serrano et al. were able to induce hydrophobic prepolymer microdomains in the elastomeric crosslinked network.[52] This resulted in thermally induced shape memory properties at room to body temperature, modulation of mechanical properties, longer degradation times, and the ability to be used with hydrophobic drugs.[52]

Silicone was also investigated as a material thanks to its long history in the medical field. The silicone elastomer matrix was optimized for the release of the model drug diclofenac. Snorradottir et al. combined excipients that had been used as enhancers with silicone to create an effective transdermal drug delivery device for diclofenac.[53] Although the enhancers showed an improved effect on drug delivery, they had a negative effect on the tensile strength of the silicone. However,

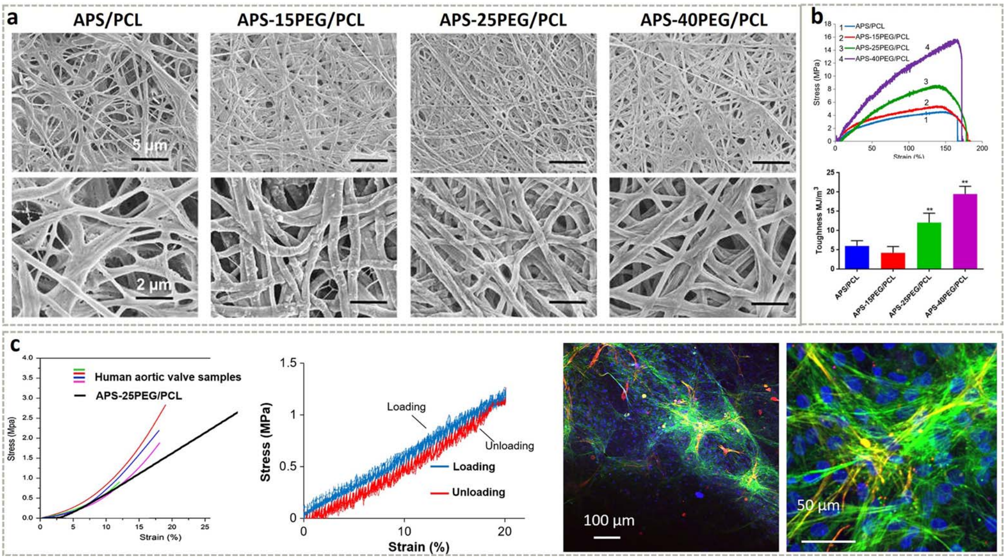

FIG. 9. — (a) Scanning electron micrographs of electrospun APS-co-PEG/PCL scaffolds. (b) Mechanical properties of electrospun APS-co-PEG/PCL scaffolds. (c) Mechanical and biological properties of electrospun APS-co-PEG/PCL scaffolds applicable to heart valve tissue engineering.[76]

testing showed that all material properties were acceptable for use in medical devices.[53] As more materials and production methods are explored, more customizability can be achieved to suit those who require periodic or continuous injections.

TISSUE SCAFFOLDING

Although controlled drug release devices serve as an external medical application of elastomers, they also show promise in the future of internal medicine such as tissue engineering. In tissue engineering, the most widely used polymers are biodegradable thermoplastic polymers. However, these materials are prone to bulk degradation in vivo, causing sudden mechanical failure. Biodegradable thermoset elastomers usually degrade by surface degradation, leading to a predictable loss of mechanical properties. When this fact is combined with elastomers' mechanical compliance, and ability to withstand cyclic loading and unloading, biodegradable thermoset elastomers prove to be the superior option.

Sant and coworkers developed an elastomeric tissue scaffold that possesses predictable degradation through the copolymerization of poly(ester amide) (PEA) and poly(ethylene glycol) (PEG).[76] Poly(1,3-diamino-2-hydroxypropane-co-glycerol sebacate) (APS-co-PEG) was synthesized from 1,3-diamino-2-hydroxy-propane (DAHP), glycerol, and sebacic acid (SA) to be used in the copolymerization with PEG. The APS-co-PEG pre-polymer was synthesized via a one-pot two-step condensation polymerization. The first step was the reaction of SA and PEG. Afterward, DAHP and glycerol were added to the reaction and mixed thoroughly to form the thermoset elastomer. The thermoset was then electrospun to form porous scaffolds (Figure 9a).

Hybrid APS/PCL and all APC-co-PEG/PCL electrospun scaffolds with proper fiber formation could be successfully fabricated. The nanofibrous structures of the electrospun scaffolds mimicked fibrous structures of native extracellular matrix (ECM) and were shown to improve the exchange of nutrients and waste products as well as promote cell attachment and spreading. The average fiber diameters of the scaffolds were ~300 nm. This proved to be desirable because the cells that form on these polymer scaffolds secrete ECM proteins that form fibrils of similar sizes. As PEG concentration was increased within the APS-co-PEG copolymer, properties such as tensile strength, elastic modulus, and toughness all increased (**Figure 9b**). In addition, mechanical properties can be further tuned by adjusting the ratio of APS-co-PEG/PCL and electrospinning parameters. In vitro degradation studies found that the scaffolds all degraded at the same rate, with a 50% mass loss after 2 weeks in PBS. The degradation of all scaffolds showed a linear trend, indicating that it was due to surface degradation. This is advantageous because the scaffolds undergo a gradual decrease in mechanical properties while maintaining their geometry, as opposed to bulk degradation that causes an abrupt structural collapse. After 2 weeks of degradation, the nanofibrous structures were maintained even after a 50% mass loss, as well as a significant reduction in mean fiber diameter. This confirms surface degradation as the primary mechanism.

The mouse cytoplast cell line C2C12 was used to evaluate the biocompatibility of different scaffolds. APS-co-PEG/PCL showed a reduction in the initial attachment of C2C12 cells, likely due to higher hydrophobicity from PEG, whereas the APS/PCL control group showed high initial cell attachment. In terms of cell proliferation, for the first 3 days, there was no distinguishable difference between APS-co-PEG/PCL and APS/PCL scaffolds. However, on day 7 APS-co-25PEG/PCL showed higher metabolic activity than all other scaffolds. Current heart valve substitutes suffer from thrombogenicity issues (blood clotting) that can lead to biomechanical mismatch and device failure. However, PEG was shown to decrease thrombogenicity in polymeric materials, making the PEGylated elastomer an excellent material for heart valve substitutes. This was tested via platelet adhesion, in which all APS-co-PEG/PCL scaffolds showed lower platelet adhesion than pure PCL and APS/PCL. In addition, the platelets in the PEGylated elastomers showed round morphology, indicating better hemocompatibility. PEGylated elastomers can also maintain scaffold integrity in dynamic conditions in the heart valve. APS-25PEG/PCL showed very similar stress–strain curves to those reported for the human aortic valve. The APS-25PEG/PCL scaffolds withstood 10 cycles of loading and unloading with minimal energy loss (**Figure 9c**). All these factors show the PEGylated elastomer's potential as a heart valve substitute material.[76] This polymeric tissue scaffold undergoes gradual degradation, thereby averting the bulk collapsing phenomenon often observed in other polymeric tissue scaffolds. In addition, the use of PEG reduces the typical blood clotting issues caused by polymer-based heart valve replacements, which decreases the chance of device failure.

Many elastomeric materials have been investigated for use in tissue scaffolding. Engineered silicone was used to 3D print structures that could be shrunk on demand following solvent treatment, allowing for a larger scale printed scaffold to be easily shrunk down to usable sizes, rather than having to print on a microscale. Davoodi et al. 3D printed silicone-based elastomeric scaffolds by using fused deposition modeling.[48] The scaffolds were subsequently treated with acetone to enable controlled shrinking. Structures with a unit cell size of 3.3 mm were reported as having pore sizes in the range of 500 μm post shrinkage.[48]

Ergene et al. developed a novel polyurethane-based biodegradable elastomer for use in skeletal muscle tissue scaffolding that could successfully proliferate myoblasts.[49] In addition, LCEs with porous architectures have been explored for use in brain tissue scaffolding. Prévôt et al. used smectic A LCE foams with a salt-leaching method to control the pore size and distribution within the elastomer with mechanical properties that closely mimic neural environments.[50]

Miceli et al. improved scaffold adhesion by incorporating dopamine into polycaprolactone-PEG-polycaprolactone–based copolymers.[77] By chemically bonding dopamine to lysine, strong adhesion to different materials was achieved after melting. The elastomer, with a reported

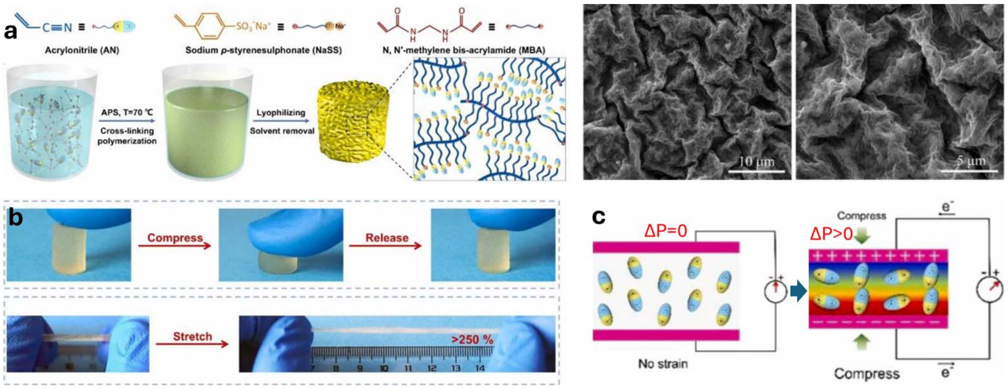

FIG. 10. — (a) Fabrication of the P(NaSS-co-AN) elastomer and its characterization. (b) Mechanical properties of the P(NaSS-co-AN) elastomer. (c) Alignment of internal dipoles under external stress.[79]

melting point of 55 °C, is deemed optimal for melt extrusion 3D printing. This characteristic facilitates the production of precise microfibers and allows for the construction of structures with tunable microarchitecture and external shape.[77] Although tissue scaffolding remains a less researched area compared to other elastomer-based projects, it still shows great promise as new elastomers are developed.

ENERGY HARVESTING

PIEZOELECTRICS

Piezoelectric materials generate charge in response to mechanical stress. Although most commonly used in the form of quartz for many materials from lighters to watches, piezoelectric polymers, such as polyvinylidene difluoride (PVDF), have been looked at for new applications.

Zhou and coworkers developed an elastic piezoelectric copolymer from polyacrylonitrile that did not utilize any ceramic or polymeric fillers.[79] The piezoelectric copolymer poly(sodium *p*-styrenesulphonate-co-acrylonitrile) [P(NaSS-co-AN)] can be prepared through a two-step process: the monomer and crosslinker are dissolved in DMSO before undergoing gelation in the presence of ammonium persulfate (APS) initiator to form an organogel. The resulting organogel was freeze-dried to remove DMSO. The final product yielded a P(NaSS-co-AN) copolymer network (Figure 10a).

P(NaSS-co-AN) showed excellent elastic properties through extensive stretching and compression without damage to the material. P(NaSS-co-AN) also showed tensile strains >250%. In addition, through the inclusion of NaSS, Young's modulus decreased to 0.16 MPa, which is comparable with that of human soft tissue. At a strain of >99%, P(NaSS-co-AN) sustained a compressive stress of 7.705 MPa without fracturing while fully recovering its height. Cyclic tensile stress tests with an applied stress of 100% showed complete self-recovery and small hysteresis (Figure 10b). The tensile stress of the following cycles were significantly greater than those of the previous cycles. This is attributed to increased dipolar interactions as the interchain distances are reduced by cyclic tensile deformation (Figure 10c). Hysteresis loops were found to be almost the same for each cycle, indicating excellent mechanical stability. However, pronounced hysteresis loops occurred at high deformations, indicating bond breaking. The voltage and current are generated through a stress-induced

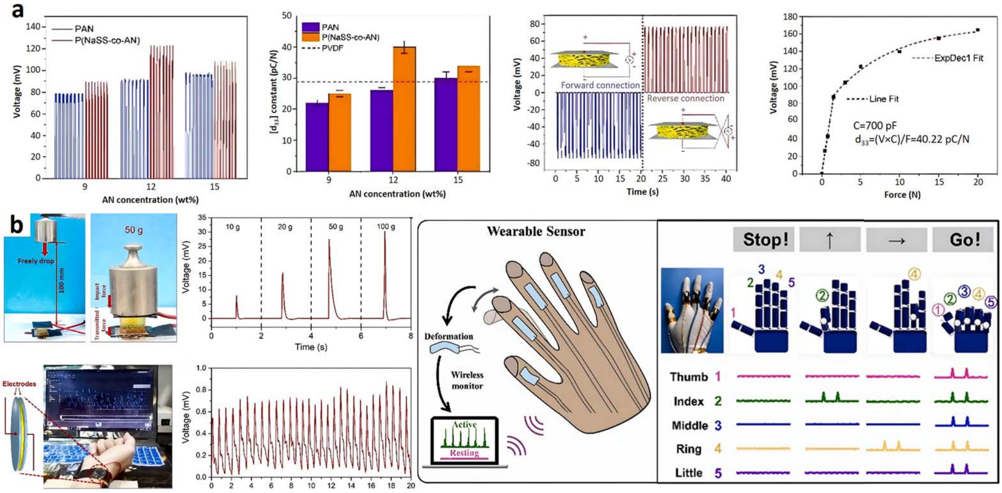

FIG. 11. — (a) Piezoelectric output properties of the P(NaSS-co-AN) elastomer. (b) Demonstrations of P(NaSS-co-AN) piezoelectric elastomer.[79]

poling effect, where internal dipoles align in a uniform direction under stress (Figure 10c). As the weight ratio of AN was increased from 9 to 12%, the output voltage also increased from 90 to 120 mV; however, the addition of more AN saw a decrease in output voltage to 110 mV (Figure 11a). This is attributed to a higher crosslinking density as AN is added, which leads to a decrease in free cyano. The maximum bulk d_{33} (deformation in the direction of the induced potential) value for P(NaSS-co-AN) was reported as 40 pC/N, which is higher than standard PVDF reported at ~29 pC/N.[78] The effect of mechanical force (F) on the output voltage (V) was measured by increasing the loading force from 0.4 to 20 N and recorded as a V-F plot (Figure 11a). The sensitivity was defined as the slope of the V-F curve, showing two regimes: a linear regime when $F < 1.5$ N and a nonlinear regime when $F > 1.5$ N. The linear regime showed a high sensitivity of 57.45 mV/N. The output signal increased with increasing thickness; however, it showed diminishing returns once it reached high levels. The piezoelectric elastomers showed an immediate electrical response to external loads. P(NaSS-co-AN) showed ultrafast response times of ~1 ms and short relaxation times at ~20 ms (Figure 11b).[79] This piezoelectric elastomer presents numerous opportunities in wearable energy harvesting, owing to its inherent elasticity. Its capacity to interpret hand signals positions it as a promising candidate for future applications in sign-to-voice technology, potentially bridging communication gaps.

Piezoelectric elastomers are most often used in resistive sensors, but have potential use for a range of innovative technologies owing to their ability to generate an electric charge from kinetic motion. A piezoelectric elastomer made of PVDF and a novel polyacrylonitrile elastic substrate was developed by Cheng et al. for use in electron skin that is soft and stretchable, while showing a high piezoelectric coefficient.[54] PDMS, PVDF, and multi-walled CNTs (MWCNTs) were mixed together to create an elastomer-based composite that was both stretchable and piezoelectric. The sensitivity of the elastomer was found to be affected by the PVDF and MWCNT content, which allows this elastomer to be customized for use as piezoresistive sensing elements.[54]

Wang et al. developed a lactate-based piezoelectric elastomer to increase the piezoelectric coefficient without having to change the dipole orientation, and possessed room temperature self-healing properties.[56] The lactate-based elastomer showed a piezoelectric short-circuit current density of 19.75 μA·cm^{-2} due to large lattice distortions and asymmetry within the polymer structure, a value 4.21 times the control elastomer. In addition, the elastomer showed fast severing healing times of 15 min at body temperature, while retaining 77.38 and 44.98% of initial mechanical and electrical properties, respectively.[56]

There has also been research into lactate-based piezoelectric generators with an overall green production cycle, opening up its use in environmentally friendly technologies. Wang et al. prepared an elastomer by the random copolymerization of lactate, 1,4-butanediol, and sebacate monomers, which resulted in a reduced elastic modulus.[57] This reduced elastic modulus, in turn, allowed for more efficient piezoelectric conversion, with a reported output voltage of 303.75 mV cm^{-2}. The elastomer also boasted biodegradability with a 36.7% weight loss over the course of 30 days in PBS.[57] Piezoelectric elastomers have strong application possibilities, with room for much more improvement.

TENGS

TENGs are similar in concept to piezoelectric materials: they both convert mechanical energy to electrical energy. However, TENGs perform under a basis of contact and separation of certain materials to create electrostatic conduction. Because of this, they have been considered for use in efficient wave energy harvesting.

Wang and coworkers successfully harvested wave energy by using a TENG with a silicone rubber/carbon black composite electrode and an integrated spring to convert low frequency motion into high-frequency vibration.[80] The segmented (cut into strips) silicone rubber/carbon black electrode was made by mixing equal volumes of Ecoflex 00-30 and carbon black. The silicone-based and spring-assisted TENG was made by taking two poly(tetrafluoroethylene) (PTFE) and depositing Cu on one side to serve as the electrodes, which were each attached to an acrylic block. The two acrylic blocks were then connected by a moderately rigid spring. An open acrylic box was fabricated to hold the spring-connected acrylic blocks, and two silicone rubber/carbon black electrodes were attached to two internal walls of the box. Finally, two TENG units with the C/PTFE-Cu triboelectric material pair were connected in parallel by using two rectifier bridges that were attached to the outer wall of the box to obtain the final TENG. The principle design is two spring-connected acrylic blocks attached by the PTFE-Cu films collide with the silicone-based electrode on the internal wall of the outer acrylic box, generating a charge (Figure 12a).

A sample with a tribo-surface area of 6 cm^2 with a separation of 5 mm reached a maximum output current of 22.3 μA and output voltage of 630.7 V. The Cu/PTFE-Cu TENG showed the lowest electrical outputs, whereas the C/PTFE-C TENG showed the highest (Figure 12b). This is attributed to the flexibility of silicone allowing better contact with the PTFE film, thereby increasing the charge transfer area. As the tribo-surface area increased, the charge and current density peak values both decreased along with the maximum power density at a matched resistance (Figure 12c). The output current and voltage, however, both increased with surface area. It was found that by segmenting the silicon rubber/carbon black electrode, the performance of the TENG was greatly enhanced, regardless of the tribo-surface area (Figure 12d). Similar to the effect of reducing the tribo-surface area, the segmented electrode allowed for better contact with the PTFE film to increase the surface charge density. For water wave energy harvesting evaluation, the maximum displacement of the external box was fixed a 7.0 cm and the maximum speed of the motor was set to 1 m/s. Both the segmented and nonsegmented TENG devices showed a gradual increase in output current with increasing motor acceleration; however, the segmented device was overall higher. The nonsegmented TENG produced a maximum output power of 10.1 mW at a matched resistance of 20 MΩ,

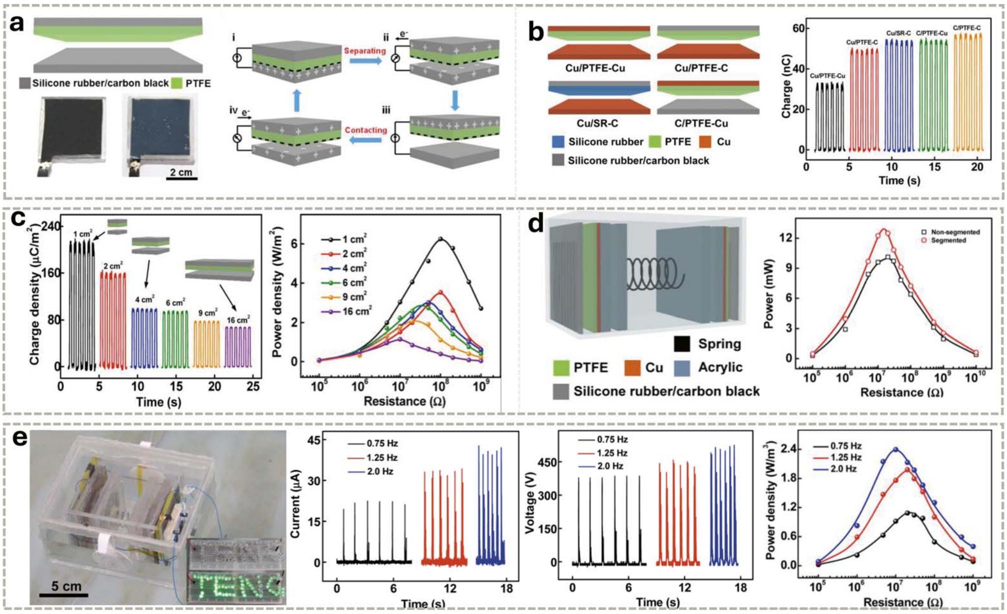

FIG. 12. — (a) Schematic of C/PTFE-C TENG device. (b) Schematic and output of TENG with different triboelectric materials. (c) Electrical properties of C/PTFE-C and Cu/PTFE-Cu TENG devices. (d) Schematic and output of silicone-based and spring-assisted TENG device. (e) Silicone-based and spring-assisted TENG device in water and wave energy harvesting output.[80]

whereas the segmented TENG produced an output power of 12.5 mW under the same conditions. Driven by the water motion, 65 light-emitting diodes (LEDs) were lit up by the device. The rectifier outputs at different water wave frequencies were then measured. It was found that with increasing frequency, output current, output voltage, and maximum peak power density all increased. The integrated device was recorded delivering a maximum current of 42.7 μA, a maximum voltage of 524.8 V, and a maximum power density of 2.4 W/m^3 at a frequency of 2 Hz (**Figure** 12e).[80] This technology ultimately serves as a means for clean energy generation from a renewable and abundant source. Because the TENG device sits on the water's surface, it is easy to install and remove as needed.

TENGs hold some mechanical energy harvesting applications beyond that of wave motion. Chen et al. used TENGs for biomotion energy harvesting through TENG fabric that takes advantage of the electrostatic breakdown phenomena of clothes.[58] The direct current fabric TENG (DC F-TENG) was made by weaving together twisted polyamide yarn and twisted conductive polyamide yarn into simple fabrics. A 1.5 cm × 3.5 cm DC F-TENG was capable of lighting up 416 LEDs, whereas a larger sample of 6.8 cm × 7 cm was reported as generating an open circuit voltage up to 4500 V.[58] Pu et al. used TENGs for human–machine interfaces (HMIs) that sense micromotion from the skin around the eyes for an eye motion-triggered HMI communication device.[59] The final device was mounted onto the arms of a pair of glasses and successfully used in a smart home control system and a hands-free typing device.[59]

A fully printable TENG was also developed by Seol et al. by using only additive two-dimensional (2D) and 3D printing methods, allowing for simple fabrication that can be done autonomously at the point of demand.[60] The structural frame was fabricated via 3D printing into a core–shell structure that converted external vibrations into continuous sliding, whereas the contact layers were fabricated via 2D inkjet printing. An unoptimized printed TENG was able to produce a maximum instantaneous voltage of 98.2 V. Other structures are also possible based on this method.[61]

Su et al. stacked elastic polyurethane and nonelastic fluororubber to fabricate a TENG with the triboelectric characteristics of both materials and the elasticity of polyurethane.[81] By stacking the conductive and nonconductive materials, contact, extrusion, and collision effects within the TENG all improved, resulting in higher performance. The final TENG achieved an instantaneous open circuit voltage of 661 V, a voltage that proved to be better than fluororubber-based and polyurethane-based TENGs combined.[81] TENGs, alongside piezoelectric elastomers, show some of the most promise for flexible energy-generating materials and will no doubt be a staple in the coming wave of technology.

CONCLUSION

In this review, we explored the remarkable versatility of rubbers and elastomers in four prominent domains: soft robotics, stretchable and wearable devices, biomedical applications, and energy harvesting. Each domain benefited from the unique properties of these materials, driving progress and innovation in their respective fields. As we look ahead, it is clear that the journey is far from over. The continued development of rubbers and elastomers holds the promise of even more groundbreaking applications. In soft robotics, we anticipate further advances in autonomous soft robots, enhancing their capabilities in tasks ranging from search and rescue to surgical procedures. Stretchable and wearable devices will continue to evolve, potentially leading to fully integrated flexible devices with enhanced durability and functionality. The convergence of electronics and materials science will play a pivotal role in shaping our future technologies. Biomedical applications will see the refinement of biocompatible elastomers, enabling the creation of more lifelike prosthetics and sophisticated medical implants. The fields of tissue engineering and regenerative medicine are poised for significant breakthroughs. Finally, energy harvesting stands as a beacon of hope for sustainable energy solutions. We can anticipate the integration of rubber-based energy harvesters into everyday products, further reducing our reliance on traditional power sources and contributing to a greener future.

However, it is important to note that these above-mentioned four domains are just a glimpse into the expansive world of rubber and elastomer applications. Beyond these representative areas, researchers are continually pushing the boundaries and discovering novel uses in fields such as smart textiles[82], and rechargeable batteries[83] to name a few.

The future of elastomers and rubbers encompasses a multitude of considerations. It is evident that elastomers will play a pivotal role in advancing technologies such as wearable devices and soft grippers. In addition, elastic conductors are highly sought after for their potential application in foldable displays. However, this review also highlights a growing emphasis on sustainability within the field. It is foreseeable that as time progresses, there will be increasing pressure for the adoption of biodegradable materials derived from renewable sources. Moreover, piezoelectric and TENGs are poised to experience heightened demand as bioenergy harvesting sources, particularly with the growing availability and use of wearable electronics. Furthermore, there is a likelihood of increased demand for their use in clean and efficient energy harvesting, as society transitions toward alternative energy sources. Although the full potential of these applications may require further development, it is reasonable to anticipate significant advancements in the not-too-distant future.

In the coming years, interdisciplinary collaboration, material design, and technological innovation will continue to propel the diverse applications of rubbers and elastomers forward. Scientists, engineers, and industries must work together to overcome challenges, ensure scalability, and unlock the full potential of these versatile materials. As we venture into this exciting future, the horizons of rubbers and elastomers in emerging technologies appear boundless, promising a world where flexibility and resilience shape our technological landscape.

ACKNOWLEDGEMENTS

The authors thank Tiantian Li and Zaili Hou for assistance in drafting this article.

REFERENCES

[1] D. Hosler, S. L. Burkett, and M. J. Tarkanian, *Science* **284**, 1988 (1999).

[2] Prescott Instruments, "History of Rubber: Development & Vulcanisation," https://www.prescott-instruments.com/history-of-rubber-development-vulcanisation/. Accessed September 9, 2023.

[3] G. B. Kauffman and R. B. Seymour, *J. Chem. Educ.* **67**, 422 (1990).

[4] H. Morawetz, RUBBER CHEM. TECHNOL. **73**, 405 (2000).

[5] American Chemical Society, "U.S. Synthetic Rubber Program," https://www.acs.org/education/whatischemistry/landmarks/syntheticrubber.html. Accessed September 9, 2023.

[6] Martin's Rubber Company, "What Is Vulcanised Rubber Used For?," https://www.martins-rubber.co.uk/blog/what-is-vulcanised-rubber-used-for/. Accessed September 9, 2023.

[7] G. B. Kauffman and R. B. Seymour, *J. Chem. Educ.* **68**, 217 (1991).

[8] The Rubber Company, https://therubbercompany.com/

[9] Greene Rubber Company, https://www.greenerubber.com/our-products/

[10] Hanna Rubber Company, https://hannarubbercompany.com/

[11] L. Marechal, P. Balland, L. Lindenroth, F. Petrou, C. Kontovounisios, and F. Bello, *Soft Robot.* **8**, 284 (2021).

[12] S. Shian, K. Bertoldi, and D. R. Clarke, *Adv. Mater.* **27**, 6814 (2015).

[13] J.-H. Youn, S. M. Jeong, G. Hwang, H. Kim, K. Hyeon, J. Park, and K.-U. Kyung, *Appl. Sci.* **10**, 640 (2020).

[14] M. Guo, Y. Wu, S. Xue, Y. Xia, X. Yang, Y. Dzenis, Z. Li, W. Lei, A. T. Smith, and L Sun, *J. Mater. Chem.* **A7**, 25969 (2019).

[15] X. Su, H. Li, X. Lai, L. Zheng, Z. Chen, S. Zeng, K. Shen, L. Sun, and X. Zeng, *ACS Appl. Mater. Interfaces* **12**, 14578 (2020).

[16] M. Park, J. Park, and U. Jeong, *Nano Today* **9**, 244 (2014).

[17] H. Stoyanov, M. Kollosche, S. Risse, R. Wache, and G. Kofod, *Adv. Mater.* **25**, 578 (2013).

[18] J. Wang, S. Yang, P. Ding, X. Cao, Y. Zhang, S. Cao, K. Zhang, S. Kong, Y. Zhou, X. Wang, D. Li, and D. Kong, *ACS Appl. Mater. Interfaces* **11**, 18590 (2019).

[19] S. Chen, H. Liu, S. Liu, P. Wang, S. Zeng, L. Sun, and L. Liu, *ACS Appl. Mater. Interfaces* **10**, 4305 (2018).

[20] W. Gao, J. Guo, J. Xiong, A. Smith and L. Sun, *Compos. Sci. Technol.* **162**, 49 (2018).

[21] Q. He, T. Yuan, X. Zhang, S. Guo, J. Liu, J. Liu, X. Liu, L. Sun, S. Wei, and Z. Guo, *Mater. Res. Express* **1**, 035029 (2014).

[22] Z. Ma, J. Zhou, J. Zhang, S. Zeng, H. Zhou, A. T. Smith, W. Wang, L. Sun, and Z. Wang, *Mater. Horiz.* **6**, 2003 (2019).

[23] C. Yu, B. Xie, X. Yao, N. Hu, J. Guo, X. Jiang, A. T. Smith, and L. Sun, *Matter* **6**, 4321 (2023).

[24] S. Zeng, R. Li, W. R. T. Tait, A. T. Smith, M. Zhang, M. Zhu, N. Chov, G. Xu, D. Zhang, and L. Sun, *Mater. Horiz.* **7**, 2368 (2020).

[25] S. Zeng, A. T. Smith, K. Shen, and L. Sun, *Acc. Mater. Res.* **3**, 1115 (2022).

[26]C. P. Ambulo, S. Tasmim, S. Wang, M. K. Abdelrahman, P. E. Zimmern, and T. H. Ware, *J. Appl. Phys.* **128**, 140901 (2020).

[27]C. Jiang, L. Zhang, Q. Yang, S. Huang, H. Shi, Q. Long, B. Qian, Z. Liu, Q. Guan, M. Liu, R. Yang, Q. Zhao, Z. You, and X. Ye, Self-healing polyurethane-elastomer with mechanical tunability for multiple biomedical applications in vivo. *Nat. Commun.* **12**, 4395 (2021).

[28]A. Lendlein and R. Langer, *Science* **296**, 1673 (2022).

[29]X. Zhang, Z. Wang, H. Jiang, H. Zeng, N. An, B. Liu, L. Sun and Z. Fan, *Sci. Adv.* **9**, eadh1415 (2023).

[30]Y. Jiang, S. Liu, M. Zhong, L. Zhang, N. Ning, and M. Tian, *Nano Energy* **71**, 104606 (2020).

[31]T. Liu, M. Liu, S. Dou, J. Sun, Z. Cong, C. Jiang, C. Du, X. Pu, W. Hu, and Z. L. Wang, *ACS Nano* **12**, 2818 (2018).

[32]D. Yurchenko, D. V. Val, Z. H. Lai, G. Gu, and G. Thomson, *Smart Mater. Struct.* **26**, 105001/1 (2017).

[33]D.-S. Choi, T.-H. Kim, S.-H. Lee, C. Pang, J. W. Bae, and S.-Y. Kim, *ACS Appl. Mater. Interfaces* **12**, 44147 (2020).

[34]Y. Hao, Z. Liu, J. Liu, X. Fang, B. Fang, S. Nie, Y. Guan, F. Sun, T. Wang, and L. Wen, *Smart Mater. Struct.* **29**, 035006 (2020).

[35]J. Hughes and F. Iida, *Soft Robot.* **5**, 512 (2018).

[36]S. Terryn, J. Brancart, D. Lefeber, G. Van Assche, and B Vanderborght, *Sci. Robot.* **2**, eaan4268 (2017).

[37]T. A. Gisby, B. M. O'Brien, and I. A. Anderson, *Appl. Phys. Lett.* **102**, 193703/1 (2013).

[38]M. O. Saed, C. P. Ambulo, H. Kim, R. De, V. Raval, K. Searles, D. A. Siddiqui, J. M. O. Cue, M. C. Stefan, M. R. Shankar, and T. H Ware, *Adv. Funct. Mater.* **29**, n/a (2019).

[39]M. Zadan, D. K. Patel, A. P. Sabelhaus, J. Liao, A. Wertz, L. Yao, and C. Majidi, *Adv. Mater.* **34**, 2200857 (2022).

[40]H. Zhao, A. M. Hussain, A. Israr, D. M. Vogt, M. Duduta, D. R. Clarke, and R. J. A. Wood, *Soft Robot.* **7**, 451–461 (2020).

[41]C.-L. He, F.-C. Liang, L. Veeramuthu, C.-J. Cho, J.-S. Benas, Y.-R. Tzeng, Y.-L. Tseng, W.-C. Chen, A. Rwei, and C.-C. Kuo, *Adv. Sci.* **8**, 2102275 (2021).

[42]H. Souri and D. Bhattacharyya, *ACS Appl. Mater. Interfaces* **10**, 20845 (2018).

[43]X. Xun, Z. Zhang, X. Zhao, B. Zhao, F. Gao, Z. Kang, Q. Liao, and Y. Zhang, *ACS Nano* **14**, 9066 (2020).

[44]Q. Li, K. Wang, Y. Gao, J. P. Tan, R. Y. Wu, and F. Z. Xuan, *Appl. Phys. Lett.* **112**, 263501/1 (2018).

[45]X. Liu, D. Liu, J.-H. Lee, Q. Zheng, X. Du, X. Zhang, H. Xu, Z. Wang, Y. Wu, X. Shen, J. Cui, Y.-W. Mai, and J.-K. Kim, *ACS Appl. Mater. Interfaces* **11**, 2282 (2019).

[46]J. Shintake, E. Piskarev, S. H. Jeong, and D. Floreano, *Adv. Mater. Technol.* **3**, 1700284 (2018).

[47]C. Tan, Z. Dong, Y. Li, H. Zhao, X. Huang, Z. Zhou, J.-W. Jiang, Y.-Z. Long, P. Jiang, T.-Y. Zhang, and B. Sun, *Nat. Commun.* **11**, 3530 (2020).

[48]E. Davoodi, H. Montazerian, A. Khademhosseini, and E. Toyserkani, *Acta Biomater.* **117**, 261 (2020).

[49]E. Ergene, B. S. Yagci, S. Gokyer, A. Eyidogan, E. A. Aksoy, and P. Y. Huri, *Biomed. Mater.* **14**, 025014 (2019).

[50]M. E. Prévôt, H. Andro, S. L. M. Alexander, S. Ustunel, C. Zhu, Z. Nikolov, S. T. Rafferty, M. T. Brannum, B. Kinsel, L. T. J. Korley, E. J. Freeman, J. A. McDonough, R. J. Clements, and E. Hegmann, *Soft Matter* **14**, 354 (2018).

[51]I. Koutsamanis, A. Paudel, C. P. Alva Zuniga, L. Wiltschko, and M. Spoerk, *J. Control. Release* **335**, 290 (2021).

[52]M. C. Serrano, L. Carbajal, and G. A. Ameer, *Adv. Mater.* **23**, 2211 (2011).

[53]B. S. Snorradottir, P. I. Gudnason, F. Thorsteinsson, and M. Masson, *Eur. J. Pharm. Sci.* **42**, 559 (2011).

[54]X. Cheng, Y. Gong, Y. Liu, Z. Wu, and X. Hu *Smart Mater. Struct.* **29**, 075007 (2020).

[55]Y. Guan, L. Tu, K. Ren, X. Kang, Y. Tian, W. Deng, P. Yu, C. Ning, R. Fu, G. Tan, and L. Zhou, *ACS Appl. Mater. Interfaces* **15**, 1736 (2023).

[56]X. Wang, Q. Liu, X. Hu, M. You, Q. Zhang, K. Hu, Q. Zhang, and Y. Xiang, *Nano Energy* **97**, 107176 (2022).

[57]X. Wang, Q. Zhang, H. Zhu, F. Wu, Y. Qiao, K. Jia, Y. Xiang, and X. Hu, *J. Mater. Sci.* **58**, 4840 (2023).

[58]C. Chen, H. Guo, L. Chen, Y.-C. Wang, X. Pu, W. Yu, F. Wang, Z. Du, and Z. L. Wang, *ACS Nano* **14**, 4585 (2020).

[59]X. Pu, H. Guo, J. Chen, X. Wang, Y. Xi, C. Hu, and Z. L. Wang, *Sci. Adv.* **3**, e1700694/1 (2017).

[60]M.-L. Seol, J.-W. Han, D.-I. Moon, K. J. Yoon, C. S. Hwang, and M. Meyyappan, *Nano Energy* **44**, 82 (2018).

[61]G. Zhao, Y. Zhang, N. Shi, Z. Liu, X. Zhang, M. Wu, C. Pan, H. Liu, L. Li, and Z. L. Wang, *Nano Energy* **59**, 302 (2019).

[62]X. Li, Q. Shi, H. Wei, X. Zhao, Z. Tong, and X. Zhu, *Biomimetics* **7**, 167 (2022).

[63]X. Zhang, W. Liao, Y. Wang, and Z. Yang, *Chem. Asian J.* **18**, e202300340 (2023).

[64]Y. Shi, E. Askounis, R. Plamthottam, T. Libby, Z. Peng, K. Youssef, J. Pu, R. Pelrine, and Q. Pei, *Science* **377**, 228 (2022).

[65]H. Liang, Y. Wu, Y. Zhang, E. Chen, Y. Wei, and Y. Ji, *Adv. Mater.* **35**, 2209853 (2023).

[66]Y. Yang, G. Zhao, X. Cheng, H. Deng, and Q. Fu, *ACS Appl. Mater. Interfaces* **13**, 14599 (2021).

[67]Z. Jiang, N. Chen, Z. Yi, J. Zhong, F. Zhang, S. Ji, R. Liao, Y. Wang, H. Li, Z. Liu, Y. Wang, T. Yokota, X. Liu, K. Fukuda, X. Chen, and T. Someya, *Nat. Electron.* **5**, 784 (2022).

[68]N. Matsuhisa, M. Kaltenbrunner, T. Yokota, H. Jinno, K. Kuribara, T. Sekitani, and T. Someya, *Nat. Commun.* **6**, 7461 (2015).

[69]H.-W. Zhu, H.-L. Gao, H.-Y. Zhao, J. Ge, B.-C. Hu, J. Huang, and S.-H. Yu, *Nano Res.* **13**, 2879 (2020).

[70]Z. Wu, Y. Guo, M. Qin, C. Liao, X. Wang, and L. Zhang, *J. Mater. Chem. A* **11**, 16074 (2023).

[71]S. Zeng, K. Shen, Y. Liu, A. P. Chooi, A. T. Smith, S. Zhai, Z. Chen, and L. Sun, *Mater. Today* **45**, 44 (2021).

[72]S. Deshmukh, E. Keaney, C. Barry, and J. Mead, RUBBER CHEM. TECHNOL. **95**, 359 (2022).

[73]S. Zeng, H. Sun, C. Park, M. Zhang, M. Zhu, M. Yan, N. Chov, E. Li, A. T. Smith, G. Xu, S. Li, Z. Hou, Y. Li, B. Wang, D. Zhang, and L. Sun, *Mater. Horiz.* **7**, 164 (2020).

[74]S. Peng, N. Thirunavukkarasu, J. Chen, X. Zheng, C. Long, X. Huang, Z. Weng, L. Zheng, H. Wang, X. Peng, and L. Wu, *Chem. Eng. J.* **463**, 142312 (2023).

[75]J. Di, S. Yao, Y. Ye, Z. Cui, J. Yu, T. K. Ghosh, Y. Zhu, and Z. Gu, *ACS Nano* **9**, 9407 (2015).

[76]Y. Xue, T. Yatsenko, A. Patel, D. B. Stolz, J. A. Phillippi, V. Sant, and S. Sant, *Polym. Adv. Technol.* **28**, 1097 (2017).

[77]G. C. Miceli, A. Martorana, F. Cancilla, G. Pitarresi, M. Licciardi, and F. S. Palumbo, *ACS Appl. Polym. Mater.* **5**, 8483 (2023).

[78]P. Martins, A. C. Lopes, and S. Lanceros-Mendez, *Prog. Polym. Sci.* **39**, 683 (2014).

[79]R. Fu, L. Tu, Y. Guan, Z. Wang, C. Deng, P. Yu, G. Tan, C. Ning, and L. Zhou, *Nano Energy* **103**, 107784 (2022).

[80]T. X. Xiao, T. Jiang, J. X. Zhu, X. Liang, L. Xu, J. J. Shao, C. L. Zhang, J. Wang, and Z. L. Wang, *ACS Appl. Mater. Interfaces* **10**, 3616 (2018).

[81]Y. Su, A. Liu, W. Feng, Y. Gu, X. Su, G. Dai, Y. Shao, L. Wan, H. Fang, and Z. Li, *ACS Omega* **8**, 18823 (2023).

[82]P. E. S. Silva, X. Lin, M. Vaara, M. Mohan, J. Vapaavuori, and E. M. Terentjev, *Adv. Mater.* **35**, 2210689 (2023).

[83]Y. Shi, N. Yang, J. Niu, S. Yang, and F. Wang, *Adv. Sci.* **9**, 2200553 (2022).

[*Received September 2023, Revised March 2024*]